Superheating of ice crystals in antifreeze protein solutions

Yeliz Celik[a], Laurie A. Graham[b], Yee-Foong Mok[b], Maya Bar[c], Peter L. Davies[b], and Ido Braslavsky[a,1]

[a]Department of Physics and Astronomy, Ohio University, Athens, OH, 45701; [b]Department of Biochemistry, Queen's University, Kingston, ON, Canada K7L3N6; and [c]Department of Structural Biology, Weizmann Institute of Science, Rehovot 76100, Israel

Edited by H. Eugene Stanley, Boston University, Boston, MA, and approved January 28, 2010 (received for review August 20, 2009)

It has been argued that for antifreeze proteins (AFPs) to stop ice crystal growth, they must irreversibly bind to the ice surface. Surface-adsorbed AFPs should also prevent ice from melting, but to date this has been demonstrated only in a qualitative manner. Here we present the first quantitative measurements of superheating of ice in AFP solutions. Superheated ice crystals were stable for hours above their equilibrium melting point, and the maximum superheating obtained was 0.44 °C. When melting commenced in this superheated regime, rapid melting of the crystals from a point on the surface was observed. This increase in melting temperature was more appreciable for hyperactive AFPs compared to the AFPs with moderate antifreeze activity. For each of the AFP solutions that exhibited superheating, the enhancement of the melting temperature was far smaller than the depression of the freezing temperature. The present findings clearly show that AFPs adsorb to ice surfaces as part of their mechanism of action, and this absorption leads to protection of ice against melting as well as freezing.

Gibbs-Thomson effect | ice recrystallization | irreversible binding | melting hysteresis | thermal hysteresis

Superheating of solids is defined as the absence of melting at temperatures higher than the equilibrium melting temperature. A solid can exist in this metastable phase up to a maximum superheating temperature at which it will lose its stability and melt catastrophically. The maximum superheating was calculated to be around 20% above the equilibrium melting temperature (1, 2). In contrast to the supercooling of liquids, which is commonly encountered, solids embedded in a liquid can rarely withstand even slight superheating because the liquid/solid interface promotes melting (1, 3, 4). Also, for crystals that are surrounded by a gas or solid, surface melting is known to occur even at temperatures below the bulk melting point (i.e., premelting) (5). Nevertheless, recent studies demonstrate that solids can be superheated if surface melting is circumvented (4, 6–9). For example, high superheating values were achieved by embedding nanocrystals of one substance into another material with a higher melting point (4, 8). Additionally, superheating inside the bulk of a material may be observed while melting occurs at the surface. For instance, superheating of ice was experimentally observed by shock heating of micron-sized crystals up to temperatures of 60 °C for 1.3 ns (10).

Knight and DeVries predicted that ice crystals in a solution containing antifreeze proteins (AFPs) would remain stable when superheated (11). They reasoned that because AFPs stop ice crystals from growing by irreversibly binding to their surfaces, such AFP adsorption should also inhibit melting. An illustration of an ice surface pinned by AFPs, with ice fronts bulging out between the AFP molecules during cooling and receding inward during heating, is shown in Movie S1. AFPs are structurally diverse proteins evolved in marine and terrestrial organisms to help survival in freezing conditions (12). They share the ability to lower the nonequilibrium freezing temperature of an ice crystal in an aqueous medium to below the melting point. This property of AFPs has been called thermal hysteresis but will be referred to here as freezing hysteresis (FH) to distinguish it from melting hysteresis (MH), which is the elevation of the nonequilibrium melting temperature above the melting point. Knight and DeVries observed the melting shape of a hole drilled in a single ice crystal (~3 cm in diameter) filled with either pure water or a solution containing AFPs (11). In the absence of AFPs, the hole remained circular during melting due to symmetrical heat flow, whereas in the presence of AFPs, the hole became asymmetrical and faceted. Additionally, they observed that melting of ice, initiated near air bubbles within the ice, tunneled toward the melted hole containing the AFP solution (11). These observations showed that the ice around the drilled hole was superheated. To date, however, no direct measurements of the superheating of ice crystals in AFP solutions have been described, and no experimental evidence has been reported showing that ice crystals can be stabilized at temperatures above the equilibrium melting point, T_m, for long periods.

Here we report measurements of the superheating of ice crystals in solutions containing hyperactive and moderately active AFPs. AFPs are classified as moderate and hyperactive according to their FH activities (13, 14). Moderate AFPs are defined here as having FH activity of 0.5 to 1.0 °C at millimolar concentrations. Hyperactive AFPs (hypAFPs) are an order of magnitude more active in FH than moderate AFPs in micromolar concentrations, and some depress the freezing point by at least 6 °C at millimolar concentrations. In the present study, the melting behavior of small ice crystals (~3–40 μm) was examined as a function of temperature and solution content. We found that ice crystals in certain AFP solutions remained stable above their equilibrium melting temperatures for up to several hours.

Results

Experiments were conducted using a custom-designed nanoliter osmometer, and samples were observed by confocal microscopy (15). We examined four hypAFPs and four moderate AFPs. These AFPs, and the abbreviations used to denote them, are summarized in Table 1.

Freezing and Melting Hysteresis. The superheating phenomenon was particularly evident during growth and melt cycles of ice crystals in solutions containing *Marinomonas primoryensis* (*Mp*AFP) (16) or *Tenebrio molitor* (*Tm*AFP) (17), both of which are hypAFPs. In Fig. 1*A*, a single ice crystal grown in *Mp*AFP solution is shown. When the temperature was dropped to a value below the FH gap of 1.87 °C, rapid ice growth propagated from the surface of the crystal (designated as "burst" growth, Fig. 1*B*). Once the sample was completely frozen, the initial crystal was still

Author contributions: Y.C., P.L.D., and I.B. designed research; Y.C., L.A.G., and Y.-F.M. performed research; M.B. contributed new reagents/analytic tools; Y.C., L.A.G., Y.-F.M., and I.B. analyzed data; and Y.C., L.A.G., P.L.D., and I.B. wrote the paper.

The authors declare no conflict of interest.

This article is a PNAS Direct Submission.

[1]To whom correspondence should be addressed at: Department of Physics and Astronomy, Ohio University, Clippinger 251, Athens, OH 45701. E-mail: braslavs@ohio.edu.

This article contains supporting information online at www.pnas.org/cgi/content/full/0909456107/DCSupplemental.

Table 1. AFPs used in the experiments; the maximum MH/FH values were measured at different protein concentrations for the different AFPs

AFP	Species	MH/FH (°C)
*Mp*AFP (hyperactive)	*Marinomonas primoryensis* (16)	0.44/2.0
*Tm*AFP (hyperactive)	*Tenebrio molitor* (17)	0.18/1.7
sbwAFP 501 (hyperactive)	Spruce budworm (18)	0.04/4.1
Dc hemolymph (hyperactive)	*Dendroides canadensis* (19)	0.20/6.2
Type II AFP (moderate)	Sea raven (20)	0.02/0.5
Type III AFP (moderate)	Ocean pout (21)	0.02/0.8
Type I AFP (moderate)	Winter flounder (22)	0.02/1.3
*Lp*AFP (moderate)	*Lolium perenne* (23)	0.00/0.8

visible and remained intact even when the sample began to melt back (Fig. 1*C*). As the temperature was raised to the T_m, all of the newly formed ice slowly melted (Fig. 1*D* and *E*). The original crystal remained intact for more than 30 min after the rest of the ice had melted. Even when the temperature was increased at a rate of 0.01 °C/30 s, the crystal did not undergo any melting until it eventually melted rapidly at 0.18 °C above T_m (Fig. 1*F*). In this instance, the MH value was roughly one-tenth of the FH value. A recording of this experiment is shown in Movie S2. These findings suggest that the ice crystal grown in AFP solution was protected from melting as well as from freezing.

Observation of Proteins Adsorbed on Ice. To visualize adsorbed proteins on ice surfaces, we tagged *Mp*AFP with green fluorescent protein (GFP). An ice crystal exposed to a 2 μM solution of the fluorescent fusion protein GFP-*Mp*AFP exhibited uniformly bright surfaces with intensely fluorescent edges, consistent with surface adsorption of the AFP (Fig. 2). When the temperature

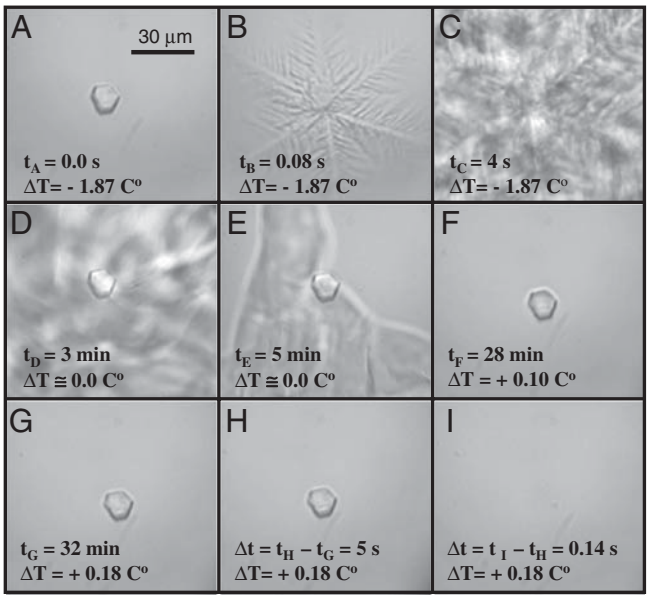

Fig. 1. Sequence of a FH and MH experiment in a drop of *Mp*AFP solution. (*A*) A single ice crystal grown in 36 μM *Mp*AFP solution was stable down to −1.87 °C below the melting point. (*B*) Dendritic growth indicating the sudden growth of the ice at this supercooling. The FH of the sample was determined as the difference between the temperature at which this dendritic growth commenced and the T_m of the sample. (*C*) Growth continued until most of the sample was frozen. (*D*–*E*) When the frozen sample was warmed to close to the melting temperature, all of the ice melted except for the initial crystal. (*F*) The remaining crystal was slowly warmed further. (*G*) The ice crystal remained stable at superheatings of up to 0.18 °C above T_m for over 25 min. (*H*) The crystal remained stable for 5 s at +0.18 °C before rapidly melting (*I*) in a 0.14 s time interval, with a velocity of 48 μm/s. The difference between the T_m and the temperature at which the crystal melted was taken as the MH.

was raised to 0.04 °C above the T_m of the crystal, the crystal melted and the bound GFP-*Mp*AFP was released into the liquid, dispersing away with a diffusion coefficient of 20 ± 10 μm^2/s. Unlike the uniform melting we observed for crystals in pure water, melting started at one point on the ice surface and then proceeded through the crystal. This can be seen in Fig. 2*F*, where melting is evident only on the left surface. Thus we consider the initiation of the melting of the surface as melting nucleation.

Melting Behavior of Ice Crystals. In some AFP solutions we observed multiple distinct ice crystals. In particular, multiple crystals readily formed at high AFP concentrations, where the crystals were stabilized faster than in low concentration solutions. Having a group of ice crystals enabled us to observe the melting nucleation of superheated ice crystals in the same droplet and gather statistical information on the melting behavior in relation to superheating. In Fig. 3*A*, the ratio of the number of crystals that had melted (N_m) relative to the initial number of crystals (N_0) as a function of superheating ($T - T_m$) is presented for a system starting with 56 crystals (5–40 μm) in a drop of 20 μM (0.18 mg/ml) *Tm*AFP solution. The temperature was increased at an average rate of 0.01 °C/7.5 s. A movie of this experiment is shown in Movie S3. The melting behavior can be fitted into a sigmoidal plot where half of the crystals melt at $\Delta T_{50\%} = 0.1$ °C. Our observation of a cumulative distribution of melting resembles experiments on crystal nucleation in which samples comprised of small separate droplets were observed (24–26). In the case of melting nucleation, the crystals can be in the same droplet due to the fact that melting of one crystal does not induce melting of a nearby crystal. A possible shortcoming of this approach is that the temperature drop associated with the melting of one crystal may influence nearby crystals. This can be explained by considering that the diffusion coefficient of heat in water is 140,000 μm^2/s (27), which means that within 0.1 s heat can diffuse to the melting crystal from hundreds of microns away. However, if the latent heat of the melting crystal and the heat capacity of the larger volume influenced by this melting are taken into account, we estimate that the temperature drop associated with the melting of a single crystal is less than 0.01 °C. This is supported by our observation that several crystals melted at around $\Delta T_{50\%}$, an unlikely event had the drop cooled significantly. In addition, the temperature-controlled stage compensates for small temperature changes within 2 s. Similar cluster melting behavior was observed in a drop of 36 μM (1.25 mg/ml) *Mp*AFP solution containing 23 ice crystals (Fig. S1).

Stability of Superheated Ice Crystals. To investigate the stability of superheated ice crystals in a drop of AFP solution, we performed experiments on a group of small ice crystals (3–24 μm in size) in 36 μM (1.25 mg/ml) *Mp*AFP solution. After the formation of the ice crystals, we slowly raised the temperature at a rate of 0.01 °C/30 s. After half of the ice crystals melted (25 out of 51), corresponding to $\Delta T_{50\%}$ of 0.22 °C above T_m, we maintained the temperature without change for 1 h. During the initial 10 min of temperature maintenance, half of the remaining crystals (13 out of the 26) melted, but further melting was not observed in the following 50 min at this temperature. Then, we slowly increased the temperature further at an average rate of 0.01 °C/8 min. During the next 3 h the crystals melted sporadically. The last ice crystal (~4 μm in size) melted at a temperature of 0.44 °C above the T_m, that is, after it was superheated for more than 4 h. The crystal size was plotted as a function of superheating and is shown in Fig. S2. This experiment suggests that there is a weak correlation between crystal size and superheating, but it is still not clear why some similarly sized crystals withstand superheating for longer periods and higher temperatures than others.

Melting Velocities of Superheated Ice Crystals. The melting behavior was further analyzed by measuring the melting velocities of ice

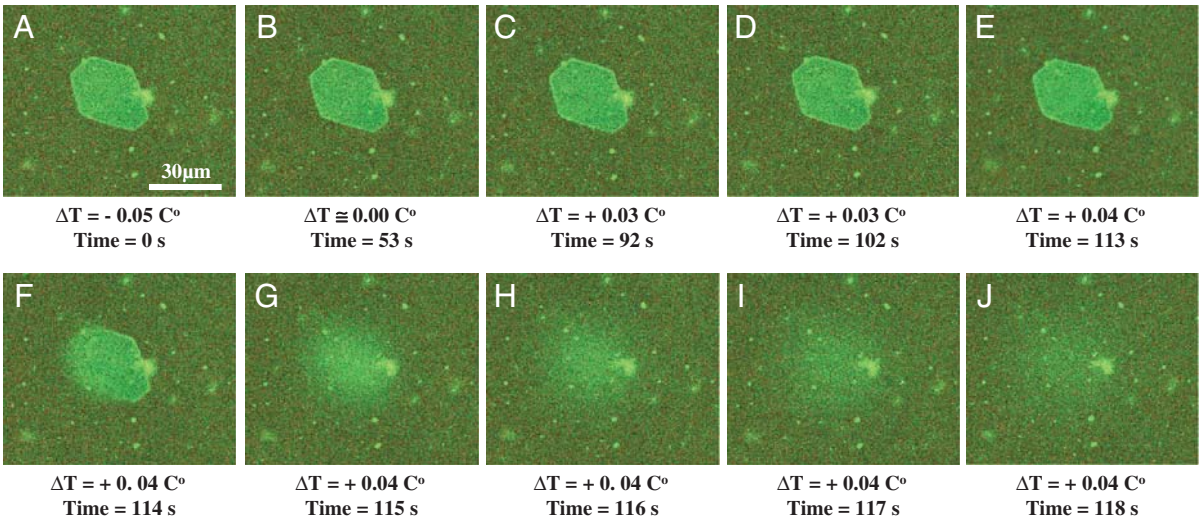

Fig. 2. Fluorescence images of ice superheated in a GFP-*Mp*AFP solution. (*A–E*) A series of images recorded while the crystal was warmed slowly to temperatures above the equilibrium melting point. (*F*) At a superheating of 0.04 °C, melting of the superheated ice crystal started at a point on the surface and proceeded through the crystal. (*G–J*) After melting commenced, the GFP-tagged AFPs that had been adsorbed on the ice diffused away.

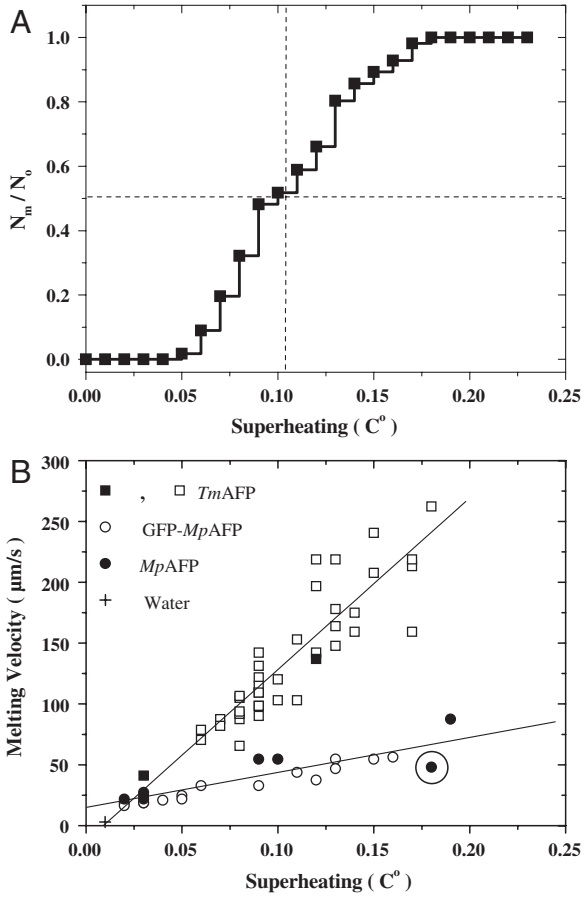

Fig. 3. Analysis of melting nucleation and the melting velocities of ice crystals formed in AFP solutions. (*A*) Cumulative fraction of melted crystals as a function of superheating in a *Tm*AFP solution. (*B*) Melting velocities of ice crystals stabilized in AFP solutions. Open squares correspond to the crystals in *A*. Solid squares represent data points from experiments using *Tm*AFP solutions with different concentrations. Note that the melting velocities recorded in multiple crystal samples were comparable to those obtained using single crystal samples. Results of additional experiments with individual crystals in *Mp*AFP (solid circles) and GFP-*Mp*AFP (open circles) solutions are also shown. The circled data point corresponds to the experiment described in Fig. 1. The melting velocity of ice in pure water at 0.01 °C is marked with the symbol +.

crystals as a function of superheating in the presence of *Tm*AFP, *Mp*AFP, or GFP-*Mp*AFP (Fig. 3*B*). The melting velocities are clearly proportional to the observed MH. For instance, when an ice crystal grown in pure water was heated to 0.01 °C above T_m, it melted with a velocity of ~3 μm/s, whereas at 0.15 °C above T_m, the superheated ice melted at velocities of 40–200 μm/s. This clearly demonstrates that the crystals are in a superheated state. In Fig. 3*B*, the line of best fit for each sample is linear and extends to a point very close to the origin. At very low superheating, however, the melting velocity may not be a linear function of superheating. It is also evident that the melting velocities are faster in the presence of *Tm*AFPs than *Mp*AFPs, indicating that the AFPs influence the melting of the ice even after melting has commenced. These findings suggest that surface kinetics and not just temperature affect the melting velocity. Nevertheless, the mechanism underlying the AFP-induced modulation of the melting velocity remains unclear.

Raman Spectroscopy of Superheated Ice. To ascertain whether there were any changes in the ice structure as the temperature was increased, we examined the crystals using Raman spectroscopy (28, 29). We did not observe any significant change in the ice spectrum as the crystal was superheated, indicating that the ice maintains its integrity and crystalline form in this state. See Figs. S3 and S4 for further details.

Melting and Freezing Hysteresis as a Function of AFP Concentration and Type. The effect of AFP concentration on both MH and FH was examined for GFP-*Mp*AFP. The FH activity showed a sigmoidal increase with a plateau at around 1.7 °C (Fig. S5), whereas the MH activity increased at a slower rate and reached a plateau at around one-tenth of the maximal FH value (Fig. 4*A*). This difference is evident in the plot of FH vs. MH in Fig. 4*B*. Similar behavior was also observed for *Dendroides canadensis* hemolymph (Fig. S6), which is a mixture of AFPs and other incompletely characterized cofactors/enhancers that exhibits extremely high antifreeze activity (30). In the present experiments we measured FH values of up to 10.5 °C. FH and MH were also measured with purified 501 isoform from the spruce budworm (sbw) AFPs (sbwAFPs) (Fig. S7). Although the 501 isoform was extremely active with a FH greater than that observed with the *Mp*AFP or the *Tm*AFP used here (13), the observed MH (Fig. S7) was far lower compared to those of *Mp*AFP and the *Tm*AFP.

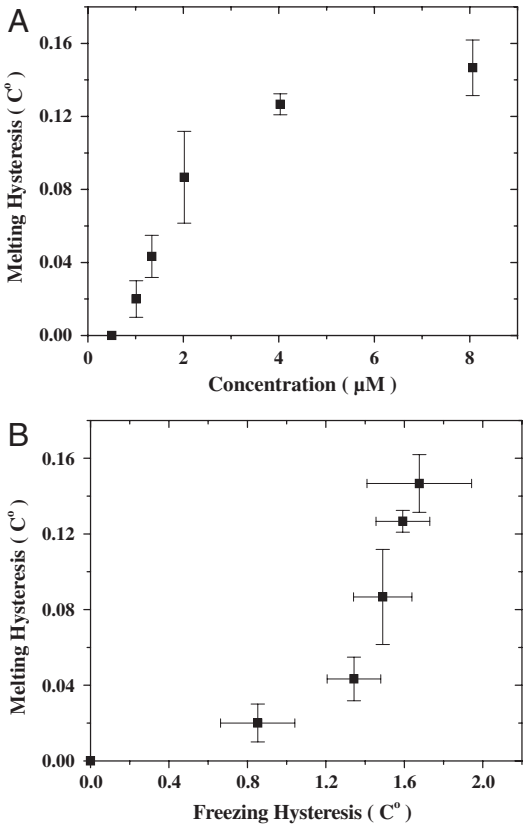

Fig. 4. Comparison of FH and MH activity for GFP-*Mp*AFP. (*A*) MH activity as a function of concentration. (*B*) The measured MH as a function of FH at the corresponding concentrations.

Finally, we conducted experiments to measure superheating in the presence of moderately active AFPs. Although all three fish AFPs tested exhibited MH, the values were lower than those observed with the hypAFPs. For example, type I AFP showed a MH of only 0.011 ± 0.003 °C, at a far higher concentration (12 mM, Fig. S8) relative to the concentrations used for the hypAFPs (Figs. S6 and S7). At lower concentrations no MH was detected for type II and III AFPs. The ice crystals melted smoothly into round shapes during a temperature increase of as little as 0.002 °C (close to the instrumental resolution, 0.001 °C) above T_m. When the temperature was lowered into the FH gap, the crystals grew into hexagonal bipyramidal shapes that could be melted back into the round shape. At higher AFP concentrations, however, type II AFP (7.1 mg/ml, 0.48 mM) and type III AFP (9 mg/ml, 1.28 mM) showed MHs of up to 0.02 °C. This may be an underestimate as it was extremely difficult to accurately measure T_m. In systems with either type I AFP or low concentrations of most of the hypAFPs mentioned above, during the initial melt, all of the crystals in the droplet decreased in size uniformly from all sides when the temperature was held at just above T_m. If the melting process was halted, even for a few seconds, it could not be resumed at the same temperature and MH was evident from the melting behavior of the crystals: The crystals melted one at a time, rapidly and nonuniformly. However, with higher concentrations of types II and III AFP as well as sbwAFP isoform 337, initial smooth melting could not be achieved; rather, the crystals melted, one at a time, rapidly and nonuniformly. This suggests that these crystals were already superheated. Once a single crystal remained, variable MH readings of up to 0.02 °C were obtained. In contrast, *Lolium perenne* (*Lp*) AFP (*Lp*AFP), which shows comparable FH activity to type I AFP, failed to show MH at concentrations up to 20 mg/mL (1.5 mM).

Discussion

Our experiments on a series of hyperactive and moderately active AFPs demonstrate that the degree of superheating of ice could be easily measured in the presence of most hypAFPs, and it is also detectable with some moderate AFPs. Given that the MHs of the hypAFPs are much lower than their FHs, it is not surprising that the MHs of the moderate AFPs are significantly lower than those of the hypAFPs, and in the case of *Lp*AFP, absent. It is also apparent that at the higher concentrations necessary for type II and III AFPs to show measurable MH activity, they appear to bind to the newly formed surfaces of the melting ice so rapidly as to affect the melt and prevent determination of accurate T_m values.

While superheating of ice in solutions containing AFPs was first discussed two decades ago (11), it has yet to become established. For instance, Kristiansen and Zachariassen argued that AFPs may not irreversibly bind to ice surfaces based on the absence of superheating of ice crystals in AFP solutions (31). According to their two-step model, AFPs bind reversibly to ice surfaces at T_m and bind irreversibly only when the temperature is dropped to values in the FH gap (31). Moreover, Zepeda et al. (32) observed that antifreeze glycoproteins (AFGPs) were not incorporated into an ice body as the ice surface slowly grew. Therefore, they concluded that AFGP adsorption must be reversible and the AFGPs do not adsorb to ice surfaces strongly. On the other hand, the model suggested by Knight and DeVries (11) to explain superheating of ice by AFGPs requires that the AFGPs attach strongly to the ice surface in order to modify the ice surface curvature and to protect the ice from melting.

One factor that has been postulated to explain the difference in FH activity between hypAFPs and moderately active fish AFPs is that while both types bind to prism or pyramidal planes, only the former binds to the basal planes (13, 15). Although ice growth or melting tends to be slower on the basal plane, a lack of binding to this surface could lead to easier melting of ice crystals (11). Indeed, Knight and DeVries suggested that AFGPs dynamically stop the basal plane growth by attaching to nearby prism planes (33). Nevertheless, other factors are doubtlessly involved as sbwAFP has been shown to bind to the basal plane (15) yet shows MH only marginally higher than that of the moderate AFPs.

According to the adsorption-inhibition model, the ice surface is pinned by AFPs and the surface curvature is directly proportional to the degree of supercooling based on the Gibbs-Thomson effect (34). Sander and Tkachenko (35) developed a theoretical explanation of the concentration dependence of FH activity based on the adsorption-inhibition model. A major parameter in their analysis is the maximum slope of the ice ($\chi_{\text{engulfment}}$) at the edge of an adsorbed AFP molecule that will resist engulfment of the AFP by the ice. If such engulfment occurs, it will result in further ice growth. A critical slope for engulfment has also been described by other groups (31, 36). Knight and DeVries (11) suggested that the AFP-induced melting inhibition should be achieved in the same manner as the freezing point depression by the Gibbs-Thomson effect but with a negative curvature between bound AFPs rather than positive. Thus, a unique critical value of the slope $\chi_{\text{superheating}} < 0$ should be determined by the resistance of the AFP molecules to leave the surface (Fig. S9). Our results clearly show that observed MH values are smaller than FH values at the same concentrations. We note that such a difference would occur if $|\chi_{\text{superheating}}|$ values are only a fraction of the corresponding $\chi_{\text{engulfment}}$ values. The increased outward curvature of the ice surface during supercooling may allow the AFP to increase its area of contact with the ice, leading to irreversible binding (37). During superheating, however, the surface would curve in the opposite direction, preventing further stabilization and perhaps allowing the AFP to desorb at a much lower curvature than that required for overgrowth. Such a difference in $\chi_{\text{engulfment}}$ and $|\chi_{\text{superheating}}|$ could account for the observation that MH is consistently lower than FH.

Several researchers consider a transition area between ice and water as continuous (32, 38) and thus do not accept the notion of irreversible attachment. One possible resolution to the different approaches could be found in recent molecular dynamic simulations of a sbwAFP (39). In the simulated system, the AFPs organized the water molecules around the ice binding face, and the mobility of the water molecules was decreased in that region. Therefore, it is reasonable to assume that the binding face of the AFP bridges through the transition layer and results in AFP attachment to the ice that gives rise to both FH and MH as described above.

The inhibition of ice melting has direct biological importance in the inhibition of ice recrystallization, which is a mechanism many organisms use to tolerate freezing. The resistance to melting, although small, will be of value particularly because it is accompanied by resistance to ice growth and will exert an effect during each of the many freeze-thaw cycles these organisms encounter during overwintering.

In conclusion, we showed that ice can be superheated in AFP solutions under isothermal conditions, and we measured the amount of superheating in the presence of moderate and hyperactive AFPs. Although AFPs were discovered more than 40 years ago, it is still unclear how they function, and suggested theories regarding their binding kinetics to ice crystals remain inconclusive. The results presented here provide strong evidence of the irreversible binding of several AFPs to ice surfaces. We hope that our results will stimulate further experimentation and theorizing and contribute to the understanding of how AFPs function at the ice/water interface. Additionally, this work implies that specific surface impurities can be used as a method to achieve superheating in solids.

Materials and Methods

Proteins. The AFPs used in this work were produced as recombinant proteins in *Escherichia coli* unless otherwise mentioned. They are as follows: the AFP domain from *Mp*AFP (16); *Tm*AFP isoform 4–9 (40); sbwAFP isoforms 337 and 501 (18); synthetic winter flounder HPLC6 (type I AFP) (22); sea raven type II AFP expressed in yeast (20); type III AFP rQAE m1.1 from ocean pout (21); the AFP domain from the perennial ryegrass (*Lp*AFP) (23). *Dendroides canadensis* larvae (19) were collected at the Queen's Biological Field Station at Lake Opinicon in late winter, their hemolymph extracted, pooled, and diluted 1:1 (vol/vol) in 50 mM Tris-HCl (pH 7.9), 150 mM NaCl, 2 mM phenylthiocarbamide with 1× concentration of complete, EDTA-free protease inhibitor (Roche Diagnostics). All the AFPs except *Tm*AFP were produced in the laboratory of Peter L. Davies (Queen's University), whereas *Tm*AFP was produced in the laboratory of Deborah Fass (Weizmann Institute of Science) (40). To conduct fluorescence microscopy studies, GFP tagged *Mp*AFP (GFP-*Mp*AFP) was expressed and purified in the laboratory of PLD in the same manner as the other tagged AFPs (41) and was not adversely affected by the fusion. Spruce budworm AFPs were kept and diluted in 20 mM Tris-HCl (pH 8). Type I, type III, and *Lp*AFP were kept and diluted in 100 mM ammonium bicarbonate (pH 8). *Tm*AFP was kept in 20 mM ammonium bicarbonate buffer (pH 8), whereas GFP-*Mp*AFP, a Ca^{2+}-dependent AFP, was kept in a buffer solution containing 20 mM $CaCl_2$ and 25 mM Tris-HCl (pH 8).

Nanoliter Osmometer Experiments. Freezing hysteresis and melting hysteresis experiments were performed using a Clifton nanoliter osmometer (Clifton Technical Physics) and a custom-designed nanoliter osmometer. Both systems were validated to give comparable results. The nanoliter osmometer experiments were conducted in a cell that has been described previously in detail (14, 42, 43). The temperature of the custom-designed nanoliter osmometer was controlled through a LabView interface developed by Ido Braslavsky. Images were recorded to a personal computer hard drive using a Sony CCD-IRIS video camera connected to a video frame grabber (IMAQ-PCI-1407, National Instruments). The images were collected at a rate of 30 frames/s.

The procedures for the measurements of thermal hysteresis values (FH and MH) were as follows: AFP solutions with submicroliter volumes were placed in immersion oil and cooled to −35 °C to induce freezing. The samples were then warmed to close to the melting point. Accurate determination of the T_m in the presence of AFPs is a challenging process due to the stabilization of ice by the proteins over short time scales, in particular at high concentrations. Thus, one should continuously melt the ice until the desired crystal size is reached. Note that the T_m depends on the osmolarity of the solution. We consider the T_m as the temperature at which the melting velocity of the last ice crystal becomes almost zero, and below that temperature the melting is halted. As an alternative method, one can consider the melting point of the buffer solution itself as a reference since the AFP concentration in the solution is low and does not significantly influence the melting point. Once the crystal of interest (10–20 μm) was formed and the melting temperature was recorded, the crystal was allowed to stabilize at a constant temperature below the T_m for 10 min. First, we performed experiments to measure the FH activity. Following the stabilization time, the temperature was decreased at a rate of 0.01 °C/4 s. The temperature at which a sudden growth burst of the crystal took place was recorded as the nonequilibrium freezing temperature, and the difference between this temperature and the melting temperature was defined as the FH activity of the protein. The procedure used for the superheating experiments was similar to that of the FH experiments up to the point where a single ice crystal was obtained.

Unless otherwise described, the following procedure was used to obtain the MH value of a sample. First, ice crystals were allowed to stabilize for 1 to 10 min at 0.3 °C below the equilibrium melting temperature. After stabilization, the temperature was increased at a rate of 0.004 to 0.02 °C/30 s. For low superheating experiments, the change of temperature was monitored with 0.001 °C resolution. Note that the temperature was measured by a thermistor that was imbedded in the metal plate with which the sample was in contact. In order to estimate the time that is needed for the ice to equilibrate down the small difference in the measured temperature, a simulation of diffusion of heat in a drop of water (300 μm in size) was conducted. The results of these computer simulations showed that the center of the drop equilibrates with its periphery in less then a second within 0.1% of the initial temperature gap. The temperature at which the superheated crystal actually melted (T_{ms}) was recorded. The difference between the T_m and the actual melting point (T_{ms}) was defined as the melting hysteresis ($MH = T_{ms} - T_m$), which can also be described as the maximum superheating of the crystal. The analysis of melting velocities at different superheating levels was performed by directly measuring the position of the surface of the ice crystal in each frame of the video recording and dividing the displacement by the elapsed time. To reduce possible size effects, only crystals smaller than 40 μm were analyzed. The small volume of the crystals and the low osmolarity of the solution ensure that there is no significant shift in the melting temperature due to changes in the osmolarity as the crystals melt. Thus, we consider that during our analyses of groups of ice crystals, the temperature measurements were not significantly affected by the melting of individual ice crystals in the same drop.

Fluorescence Microscopy Experiments. The experimental cell used in the fluorescence microscopy experiments was the same as that used in the nanoliter osmometer experiments, except that the samples were sandwiched between two cover glasses rather than placed in immersion oil. The cover glasses were sealed together with polydimethylsiloxane (Sylgard 184, Dow Corning Corp.) which was prepared with a ratio of 1:10 [vol/vol] between the curing agent and the base (41). The sandwiched cover glass was placed on a metal plate to control its temperature. Imaging was conducted through 125-μm-diameter holes in the metal plate. The size of the holes was chosen in order to be sufficiently small to ensure a low temperature gradient, but big enough to maintain good optical quality. The samples were imaged with a confocal microscope (Zeiss LSM 510) with illumination of a 488 nm argon laser line and 543 nm and 633 nm HeNe laser lines, and filters for detection of GFP and Cyanine 5 (Cy5). Cy5 was added to the sample solution to enhance the contrast between the ice-bound proteins and the proteins in solution. Previously we have shown that Cy5 does not interact with ice (14).

Raman Spectroscopy Experiments. We performed Raman spectroscopy of superheated ice as detailed in *SI Text*.

ACKNOWLEDGMENTS. The authors are grateful to S. Gauthier for her assistance in preparing AFPs and to C. Garnham and J. Whitney for tagging *Mp*AFP with GFP and to Prof. H. Richardson and A. Khan for their help with Raman spectroscopy. We thank Prof. Deborah Fass (Weizmann Institute of Science, Rehovot, Israel) for her help in the preparation of the *Tm*AFP protein. This work has been supported by the National Science Foundation (NSF) under Grant CHE-0848081 (cofunded by the MPS/CHE and the MCB divisions, and by the OISE and OPP units), the Canadian Institutes for Health Research (CIHR), the Condensed Matter and Surface Science program at Ohio University (CMSS), and the Biomimetic Nanoscience and Nanoscale Technology initiative (BNNT) at Ohio University.

1. Mei QS, Lu K (2007) Melting and superheating of crystalline solids: From bulk to nanocrystals. *Prog Mater Sci* 52(8):1175–1262.
2. Lu K, Li Y (1998) Homogeneous nucleation catastrophe as a kinetic stability limit for superheated crystal. *Phys Rev Lett* 80(20):4474–4477.
3. Vega C, Martin-Conde M, Patrykiejew A (2006) Absence of superheating for ice I_h with a free surface: A new method of determining the melting point of different water models. *Mol Phys* 104(22–24):3583–3592.
4. Xu Q, et al. (2006) Large melting-point hysteresis of Ge nanocrystals embedded in SiO_2. *Phys Rev Lett* 97(20):155701.
5. Dash JG, Fu HY, Wettlaufer JS (1995) The premelting of ice and its environmental consequences. *Rep Prog Phys* 58(1):115–167.
6. Schmeisser M, Iglev H, Laubereau A (2007) Bulk melting of ice at the limit of superheating. *J Phys Chem B* 111(38):11271–11275.
7. Wunderlich B (2007) One hundred years research on supercooling and superheating. *Thermochim Acta* 461(1–2):4–13.
8. Banhart F, Hernandez E, Terrones M (2003) Extreme superheating and supercooling of encapsulated metals in fullerenelike shells. *Phys Rev Lett* 90(18):185502.
9. Toda A, Hikosaka M, Yamada K (2002) Superheating of the melting kinetics in polymer crystals: A possible nucleation mechanism. *Polymer* 43(5):1667–1679.
10. Schmeisser M, Iglev H, Laubereau A (2007) Maximum superheating of bulk ice. *Chem Phys Lett* 442(4–6):171–175.
11. Knight CA, DeVries AL (1989) Melting inhibition and superheating of ice by an antifreeze glycopeptide. *Science* 245(4917):505–507.
12. Yeh Y, Feeney R (1996) Antifreeze proteins: Structures and mechanisms of function. *Chem Rev* 96(2):601–617.
13. Scotter A, et al. (2006) The basis for hyperactivity of antifreeze proteins. *Cryobiology* 53(2):229–239.
14. Pertaya N, et al. (2007) Growth–melt asymmetry in ice crystals under the influence of spruce budworm antifreeze protein. *J Phys: Condens Matter* 19:412101.
15. Pertaya N, Marshall CB, Celik Y, Davies PL, Braslavsky I (2008) Direct visualization of spruce budworm antifreeze protein interacting with ice crystals: Basal plane affinity confers hyperactivity. *Biophys J* 95(1):333–341.
16. Gilbert J, Davies P, Laybourn-Parry J (2005) A hyperactive, Ca^{2+}-dependent antifreeze protein in an Antarctic bacterium. *FEMS Microbiol Lett* 245(1):67–72.
17. Graham LA, Liou YC, Walker VK, Davies PL (1997) Hyperactive antifreeze protein from beetles. *Nature* 388(6644):727–728.
18. Doucet D, Tyshenko MG, Davies PL, Walker VK (2002) A family of expressed antifreeze protein genes from the moth, Choristoneura fumiferana. *Eur J Biochem* 269(1):38–46.
19. Duman JG (1984) Thermal hysteresis antifreeze proteins in the midgut fluid of overwintering larvae of the beetle *Dendroides canadensis*. *J Exp Zool* 230(3):355–361.
20. Gronwald W, et al. (1998) The solution structure of type II antifreeze protein reveals a new member of the lectin family. *Biochemistry* 37(14):4712–4721.
21. Chao H, Davies PL, Sykes BD, Sonnichsen FD (1993) Use of proline mutants to help solve the NMR solution structure of type III antifreeze protein. *Protein Sc* 2(9):1411–1428.
22. Sicheri F, Yang DSC (1995) Ice-binding structure and mechanism of an antifreeze protein from winter flounder. *Nature* 375(6530):427–431.
23. Sidebottom C, et al. (2000) Phytochemistry: Heat-stable antifreeze protein from grass. *Nature* 406(6793):256–256.
24. Massa MV, Carvalho JL, Dalnoki-Veress K (2003) Direct visualisation of homogeneous and heterogeneous crystallisation in an ensemble of confined domains of poly(ethylene oxide). *Eur Phys J E* 12(1):111–117.
25. Vali G (1971) Quantitative evaluation of experimental results on the heterogeneous freezing nucleation of supercooled liquids. *J Atmos Sci* 28(3):402–409.
26. Stan C, et al. (2009) A microfluidic apparatus for the study of ice nucleation in supercooled water drops. *Lab Chip* 9(16):2293–2305.
27. Shibkov AA, Zheltov MA, Korolev AA, Kazakov AA, Leonov AA (2005) Crossover from diffusion-limited to kinetics-limited growth of ice crystals. *J Cryst Growth* 285(1–2):215–227.
28. Richardson HH, et al. (2006) Thermooptical properties of gold nanoparticles embedded in ice: Characterization of heat generation and melting. *Nano Lett* 6(4):783–788.
29. Andreeva NP, Bunkin AF, Pershin SM (2002) Deformation of the Raman scattering spectrum of Ih ice under local laser heating near 0°C. *Opt Spectrosc (Transl of Opt Spektrosk)* 93(2):252–256.
30. Wang L, Duman JG (2005) Antifreeze proteins of the beetle *Dendroides canadensis* enhance one another's activities. *Biochemistry* 44(30):10305–10312.
31. Kristiansen E, Zachariassen KE (2005) The mechanism by which fish antifreeze proteins cause thermal hysteresis. *Cryobiology* 51(3):262–280.
32. Zepeda S, Yokoyama E, Uda Y, Katagiri C, Furukawa Y (2008) In situ observation of antifreeze glycoprotein kinetics at the ice interface reveals a two-step reversible adsorption mechanism. *Cryst Growth Des* 8(10):3666–3672.
33. Knight CA, DeVries AL (2009) Ice growth in supercooled solutions of a biological "antifreeze", AFGP 1–5: An explanation in terms of adsorption rate for the concentration dependence of the freezing point. *Phys Chem Chem Phys* 11(27):5749–5761.
34. Knight CA, Cheng CC, DeVries AL (1991) Adsorption of alpha-helical antifreeze peptides on specific ice crystal surface planes. *Biophys J* 59(2):409–418.
35. Sander LM, Tkachenko AV (2004) Kinetic pinning and biological antifreezes. *Phys Rev Lett* 93(12):128102.
36. Knight CA, Wierzbicki A (2001) Adsorption of biomolecules to ice and their effects upon ice growth. 2. A discussion of the basic mechanism of "antifreeze" phenomena. *Cryst Growth Des* 1(6):439–446.
37. Wierzbicki A, Knight CA, Salter EA, Henderson CN, Madura JD (2008) Role of nonpolar amino acid functional groups in the surface orientation-dependent adsorption of natural and synthetic antifreeze peptides on ice. *Cryst Growth Des* 8(9):3420–3429.
38. Wierzbicki A, et al. (2007) Antifreeze proteins at the ice/water interface: Three calculated discriminating properties for orientation of type I proteins. *Biophys J* 93(5):1442–1451.
39. Nutt DR, Smith JC (2008) Dual function of the hydration layer around an antifreeze protein revealed by atomistic molecular dynamics simulations. *J Am Chem Soc* 130(39): 13066–13073.
40. Bar M, Bar-Ziv R, Scherf T, Fass D (2006) Efficient production of a folded and functional, highly disulfide-bonded beta-helix antifreeze protein in bacteria. *Protein Expres Purif* 48(2):243–252.
41. Pertaya N, et al. (2007) Fluorescence microscopy evidence for quasi-permanent attachment of antifreeze proteins to ice surfaces. *Biophys J* 92(10):3663–3673.
42. Bar M, Celik Y, Fass D, Braslavsky I (2008) Interactions of beta-helical antifreeze protein mutants with ice. *Cryst Growth Des* 8(8):2954–2963.
43. Chakrabartty A, Hew CL (1991) The effect of enhanced alpha-helicity on the activity of a winter flounder antifreeze polypeptide. *Eur J Biochem* 202(3):1057–1063.